Monochromatization of femtosecond XUV light pulses with the use of reflection zone plates

Jan Metje,[1,2] **Mario Borgwardt,**[1,2] **Alexandre Moguilevski,**[1,2] **Alexander Kothe,**[1,2] **Nicholas Engel,**[1,2] **Martin Wilke,**[1,2] **Ruba Al-Obaidi,**[1,2] **Daniel Tolksdorf,**[1,2] **Alexander Firsov,**[3] **Maria Brzhezinskaya,**[3] **Alexei Erko,**[3] **Igor Yu. Kiyan,**[1,2] **and Emad F. Aziz,**[1,2,4*]

[1]*Joint Ultrafast Dynamics Lab in Solutions and at Interfaces (JULiq) Helmholtz-Zentrum Berlin, Albert-Einstein-Str. 15, 12489 Berlin, Germany*
[2]*Freie Universität Berlin, FB Physik, Arnimallee 14, 14195 Berlin, Germany*
[3]*Institute for Nanometer Optics and Technology, Helmholtz-Zentrum Berlin, Albert-Einstein-Str. 15, 12489 Berlin, Germany*
[4]*emad.aziz@fu-berlin.de*

[*] *emad.aziz@helmholtz-berlin.de*

Abstract: We report on a newly built laser-based tabletop setup which enables generation of femtosecond light pulses in the XUV range employing the process of high-order harmonic generation (HHG) in a gas medium. The spatial, spectral, and temporal characteristics of the XUV beam are presented. Monochromatization of XUV light with minimum temporal pulse distortion is the central issue of this work. Off-center reflection zone plates are shown to be superior to gratings when selection of a desired harmonic is carried out with the use of a single optical element. A cross correlation technique was applied to characterize the performance of the zone plates in the time domain. By using laser pulses of 25 fs length to pump the HHG process, a pulse duration of 45 fs for monochromatized harmonics was achieved in the present setup.

OCIS codes: (050.1965) Diffractive lenses; (190.4160) Multiharmonic generation.

References and links

1. A. Tehlar and H. J. Wörner, "Time-resolved high-harmonic spectroscopy of the photodissociation of CH_3I and CF_3I," Mol. Phys. **111,** 2057–2067 (2013).
2. P. Limão-Vieira, S. Eden, P. A. Kendall, N. J. Mason, A. Giuliani, J. Heinesch, M.-J. Hubin-Franskin, J. Delwich, and S. V. Hoffmann, "An experimental study of SF_5CF_3 by electron energy loss spectroscopy, VUV photo-absorption and photoelectron spectroscopy," Int. J. Mass. Spectrom. **233,** 335–341 (2004).
3. B. Ahr, M. Chollet, B. Adams, E. M. Lunny, C. M. Laperle, and C. Rose-Petruck, "Picosecond X-ray absorption measurements of the ligand substitution dynamics of $Fe(CO)_5$ in ethanol," Phys. Chem. Chem. Phys. **13,** 5590–5595 (2011).
4. M. Faubel, K. R. Siefermann, Y. Liu, and B. Abel, "Ultrafast soft X-ray photoelectron spectroscopy at liquid water microjets," Accounts Chem. Res. **45,** 120–130 (2011).
5. M. Krikunova, T. Maltezopoulos, P. Wessels, M. Schlie, A. Azima, and M. Wieland, "Ultrafast photofragmentation dynamics of molecular iodine driven with timed XUV and near-infrared light pulses," J. Chem. Phys. **134,** 02313 (2011).
6. L. Nugent-Glandorf, M. Scheer, D. A. Samuels, A. M. Mulhisen, E. R. Grant, X. Yang, V. M. Bierbaum, and S. R. Leone, "Ultrafast time-resolved soft X-Ray photoelectron spectroscopy of dissociating Br_2," Phys. Rev. Lett. **87,** 193002 (2001).

7. H. Soifer, P. Botheron, D. Shafir, A. Diner, O. Raz, B. D. Bruner, Y. Mairesse, B. Pons, and N. Dudovich, "Near-threshold high-order harmonic spectroscopy with aligned Molecules," Phys. Rev. Lett. **105,** (2010).
8. K. R. Siefermann, Y. Liu, E. Lugovoy, O. Link, M. Faubel, U. Buck, B. Winter, and B. Abel, "Binding energies, lifetimes and implications of bulk and interface solvated electrons in water," Nature Chem. **2,** 274–279 (2010).
9. P. Wernet, M. Odelius, K. Godehusen, J. Gaudin, O. Schwarzkopf, and W. Eberhardt, "Real-Time Evolution of the Valence Electronic Structure in a Dissociating Molecule," Phys. Rev. Lett. **103,** 013001 (2009).
10. P. Billaud, M. Géléoc, Y. J. Picard, K. Veyrinas, J. F. Hergott, S. Marggi Poullain, P. Breger, T. Ruchon, M. Roulliay, F. Delmotte, F. Lepetit, A. Huetz, B. Carré, and D. Dowek, "Molecular frame photoemission in dissociative ionization of H-2 and D-2 induced by high harmonic generation femtosecond XUV pulses," J. Phys. B-At. Mol. Opt. **45,** 194013 (2012).
11. E. R. Hosler and S. R. Leone, "Characterization of vibrational wave packets by core-level high-harmonic transient absorption spectroscopy," Phys. Rev. A **88,** 023420 (2013).
12. R. A. Dilanian, B. Chen, G. J. Williams, H. M. Quiney, K. A. Nugent, S. Teichmann, P. Hannaford, L. V. Dao, and A. G. Peele, "Diffractive imaging using a polychromatic high-harmonic generation soft-x-ray source," J. App. Phys. **106,** 023110 (2009).
13. R. L. Sandberg, C. Song, P. W. Wachulak, D. A. Raymondson, A. Paul, B. Amirbekian, E. Lee, A. E. Sakdinawat, C. La-O-Vorakiat, M. C. Marconi, C. S. Menoni, M. M. Murnane, J. J. Rocca, H. C. Kapteyn, and J. Miao, "High numerical aperture tabletop soft X-ray diffraction microscopy with 70-nm resolution," Proc. Nat. Acad. Sci. USA. **105,** 24–27 (2008).
14. R. Reininger, D. J. Keavney, M. Borland, and L. Young, "Optical design of the short pulse soft X-ray spectroscopy beamline at the advanced photon source," J. Synch. Rad. **20,** 654–659 (2013).
15. P. Radcliffe, S. Düsterer, A. Azima, H. Redlin, J. Feldhaus, J. Dardis, K. Kavanagh, H. Luna, J. Pedregosa Gutierrez, P. Yeates, E. T. Kennedy, J. T. Costello, A. Delserieys, and C. L. S. Lewis, "Single-shot characterization of independent femtosecond extreme ultraviolet free electron and infrared laser pulses," Phys. Rev. Lett. **90,** 131108 (2007).
16. P. B. Corkum, "Plasma perspective on strong-field multiphoton ionization," Phys. Rev. Lett. **71,** 1994–1997 (1993).
17. P. Salières and M. Lewenstein, "Generation of ultrashort coherent XUV pulses by harmonic conversion of intense laser pulses in gases: towards attosecond pulses," Meas. Sci. Technol. **12,** 1818 (2001).
18. X. He, M. Miranda, J. Schwenke, O. Guilbaud, T. Ruchon, C. Heyl, E. Georgadiou, R. Rakowski, A. Persson, M. B. Gaarde, and A. L'Huillier, "Spatial and spectral properties of the high-order harmonic emission in argon for seeding applications," Phys. Rev. A **79,** 063829 (2009).
19. J. Hüve, T. Haarlammert, T. Steinbrück, J. Kutzner, G. Tsilimis, and H. Zacharias, "High-flux high harmonic soft X-ray generation up to 10 kHz repetition rate," Opt. Commun. **266,** 261-265 (2006).
20. P. Villoresi "Compensation of optical path lengths in extreme-ultraviolet and soft X-ray monochromators for ultrafast pulses," Appl. Opt. **38,** 6040–6049 (1999).
21. L. Nugent-Glandorf, M. Scheer, D. A. Samuels, V. Bierbaum, and S. R. Leone, "A laser-based instrument for the study of ultrafast chemical dynamics by soft X-ray-probe photoelectron spectroscopy," Rev. Sci. Inst. **73,** 1875 (2002).
22. L. Poletto, P. Villoresi, F. Frasetto, F. Calegari, F. Ferrari, M. Lucchini, G. Sansone, and M. Nisoli, "Time-delay compensated monochromator for the spectral selection of extreme-ultraviolet high-order laser harmonics," Rev. Sci. Inst. **80,** 123109 (2009).
23. M. Ito, Y. Kataoka, T. Okamoto, M. Yamashita, and T. Sekikawa, "Spatiotemporal characterization of single-order high harmonic pulses from time-compensated toroidal-grating monochromator," Opt. Express **18,** 6071–6078 (2010).
24. J. Gaudin, S. Rehbein, P. Guttmann, S. Godé, G. Schneider, P. Wernet, and W. Eberhardt, "Selection of a single femtosecond high-order harmonic using a zone plate based monochromator," J. App. Phys. **104,** 033112 (2008).
25. P. Siffalovic, M. Drescher, M. Spiewec, T. Wiesenthal, Y. C. Lim, R. Weidner, A. Elizarov, and U. Heinzmann, "Laser-based apparatus for extended ultraviolet femtosecond time-resolved photoemission spectroscopy," Rev. Sci. Inst. **72,** 30–35 (2001).
26. V.V. Aristov, A. I. Erko, and V. V. Martynov, "Principles of Bragg-Fresnel multilayer optics," Rev. Phys. Appl. **23,** 1623–1630 (1988).
27. M. Brzhezinskaya, A. Firsov, K. Holldack, T. Kachel, R. Mitzner, N. Pontius, J. S. Schmidt, M. Sperling, C. Stamm, A. Fröhlisch, and A. Erko, "A novel monochromator for experiments with ultrashort X-ray pulses," J. Synch. Rad. **20,** 522–530 (2013).
28. M. Ibek, T. Leitner, A. Erko, A. Firsov, and P. Wernet, "Monochromatizing and focussing femtosecond high-order harmonic radiation with one optical element," Rev. Sci. Inst. **84,** 103102 (2013).
29. A. Kothe, J. Metje, M. Wilke, A. Moguilevski, N. Engel, R. Al-Obaidi, C. Richter, R. Golnak, I. Yu. Kiyan, and E. F. Aziz, "Time-of-flight electron spectrometer for a broad range of kinetic energies," Rev. Sci. Inst. **84,** 023106 (2013).
30. V. V. Aristov, S. V. Gaponov, V. M. Genkin, Yu. A. Goratov, A. I. Erko, V. V. Martynov, L. A. Matveev, N. N. Salashchenko, and A. A. Fraerman, "Focusing properties of shaped multilayer mirrors," J. Exp. Theor. Phys. **44,**

265–267 (1986).
31. Yu. A. Basov, D. V. Roshchupkin, and A. E. Yakshin, "Grazing incidence phase Fresnel zone plate for X-ray focusing," Opt. Commun. **109,** 324–327 (1994).
32. T. Wilhein, D. Hambach, B. Niemann, M. Berglund, L. Rymell, and H. M. Hertz, "Off-axis reflection zone plate for quantitative soft x-ray source characterization," Appl. Phys. Lett. **71,** 190–192 (1997).
33. Yu. A. Basov, D. V. Roshchupkin, I. A. Schelokov, and A. E. Yakshin, "2-dimensional X-ray focusing by a phase Fresnel zone plate at grazing incidence," Opt. Commun. **114,** 9–12 (1995).
34. F. Schaefers and M. Krumrey, "BESSY Technical report," (1996).
35. A. Firsov, A. I. Erko, and A. Svintsov, "Design and fabrication of the diffractive X-ray optics at BESSY," "Design and microfabrication of novel X-ray optics," A. A. Snigirev and D. C. Mancini; Eds. Proc. SPIE **5539,** 160–164 (2004).
36. A. Kramida, Yu. Ralchenko, J. Reader, and NIST ASD Team (2013). NIST Atomic Spectra Database (version 5.1), [Online]. Available: http://physics.nist.gov/asd [Friday, 15-Nov-2013 14:41:14 EST].
37. J. M. Schins, P. Breger, P. Agostini, R. C. Constantinescu, H. G. Muller, A. Bouhal, G. Grillon, A. Antonetti, and A. Mysyrowicz, "Cross-correlation measurements of femtosecond extreme-ultraviolet high-order harmonics," J. Opt. Soc. Am. B **13,** 197–200 (1996).
38. T. E. Glover, R. W. Schoenlein, A. H. Chin, and C. V. Shank, "Observation of laser assisted photoelectric effect and femtosecond high-order harmonic radiation," Phys. Rev. Lett. **79,** 2468–2471 (1996).
39. N. B. Delone, S. P. Goreslavsky, and V. P. Krainov, "Quasiclassical dipole matrix elements for atomic continuum states," J. Phys. B-At. Mol. Opt. **22,** 2941–2945 (1989).
40. P. Wernet, J. Gaudin, K. Godehusen, O. Schwarzkopf, and W. Eberhardt, "Femtosecond time-resolved photoelectron spectroscopy with a vacuum-ultraviolet photon source based on laser high-order harmonic generation," Rev. Sci. Inst. **82,** 063114 (2011).

1. Introduction

Short light pulses in the extreme ultraviolet (XUV) range find a wide variety of applications in studies on electronic and structural dynamics of molecules and molecular complexes [1–3]. In particular, photoelectron spectroscopy with the use of XUV radiation is a powerful method to probe the electron density in a valence shell of a molecular system. In combination with a pump-probe technique, this method enables to reveal mechanisms of molecular processes, which typically occur on the subpicosecond or femtosecond time scale. Recently, XUV photoelectron spectroscopy was developed for studying molecular dynamics in the liquid phase, which represents a natural environment for many interesting processes in chemistry and biology [4, 5].

The modern femtosecond laser technology provides the possibility to develop XUV light sources with such an ultrashort pulse duration via upconverting the laser frequency in the process of high-order harmonic generation (HHG) induced in a gas medium. Nowadays the HHG technique represents an established method to generate XUV radiation and is used in a variety of different research areas such as photoelectron spectroscopy [6–10], transient absorption spectroscopy [11], diffractive imaging [12] and microscopy [13]. With this tabletop technique, it is possible to achieve a femtosecond XUV-pulse duration, which is by orders of magnitude shorter than the typical pulse duration of synchrotron radiation [14] and is comparable to the pulse length of a free-electron laser [15]. The great advantage of using the HHG method in a pump-probe experiment is that the pump and the XUV-probe pulses are intrinsically synchronized, since typically the same laser system is used to generate both pules. In the present work we report on our newly built HHG setup designed for time-resolved studies on electronic and structural dynamics of molecular complexes in solutions and at interfaces.

The HHG process in an atomic gas is well understood on a fundamental level and is described in detail in literature [16–18]. It consists in a nonlinear response of atoms to the strong laser field, which involves absorption of several laser photons by a single atom and emission of one photon with the cumulated energy under relaxation of the atom to its initial ground state. In the range of higher harmonics, the envelope of the HHG energy spectrum exhibits a plateau extending up to a well-known cutoff energy [16]. As an example, HHG spectra extending up to

photon energies of 100 eV were achieved in Ref. [19] by pumping noble gases with femtosecond Ti:sapphire laser pulses of $10^{14} - 10^{15}$ W/cm^2 peak intensity.

To conduct spectroscopic studies, a single harmonic of desired photon energy needs to be selected from the HHG spectrum. Monochromatization of XUV light represents a subject of particular interest in the present work. It becomes a challenging task when a short XUV pulse is required, since the use of dispersive optics required for energy resolution introduces temporal broadening. This distortion is defined by the total difference in the optical paths of the rays. In a grating monochromator it can easily reach several hundred femtoseconds or even a picosecond, e.g., when 10^4 grooves are illuminated by XUV light of 30 nm wavelength. This represents a dramatic value. The time dispersion can be significantly compensated with the use of a second grating [20,21]. The two-grating monochromator developed in [22] enabled to reduce the XUV pulse duration down to 8 fs. However, a setup with two gratings causes significant losses in the transmission efficiency and complicates handling of the beam pass through the monochromator [23]. Some other methods for the selection of harmonics which are based on using transmission zone plates [24] and narrow-band multilayer mirrors [25] were reported. While a time resolution in the order of 100 fs could be achieved with the use of multilayer mirrors, the disadvantage of these methods is a poor spectral resolution.

In the present work, we explore the advantage of using an off-axis reflection zone plate (ZP) for the purpose of harmonics selection. The basic principles of this optical element were formulated in [26]. Similar to a toroidal grating, an off-axis ZP diffracts different spectral components of the incident beam at different angles and focuses them into spatially separated spots. The zone structure can be designed such that a given spectral component has a minimal temporal distortion and a sufficient spatial separation from other components in the focal plane. Recently, the application of ZPs has been developed as a novel method of handling synchrotron beams in the X-ray energy range. In particular, it has been successfully used at the femtosecond slicing beam line of BESSY II [27]. The potential of using ZPs for the selection of high harmonics was recently discussed in [28]. Below we describe our newly built HHG setup which implements off-center reflection zone plates for monochromatization of the femtosecond XUV pulses generated in argon. We will present the time-resolution characteristics of the monochromator measured using a cross-correlation technique. To our knowledge this is the first performance test of reflection zone plates in the time domain.

2. Experimental setup

2.1. Generation of XUV light

A femtosecond Ti:sapphire laser system operated at 5 kHz repetition rate was used to generate high harmonics in a gas cell filled with argon. The laser output of 2.5 mJ pulse energy had a pulse length of 25 fs at a central wavelength of 800 nm. Laser pulses were split into two beams by a beam splitter so that an energy of up to 1.5 mJ per pulse was used to pump the HHG process. The other split beam is dedicated for future pump-probe experiments. In the present work it was used in the cross-correlation experiment to characterize the XUV pulse duration.

A schematic view of the experimental setup is shown in Fig. 1. Laser pulses were focused with a lens of 600 mm focal length into a gas cell which was filled with argon and positioned in a vacuum chamber. An iris aperture and a $\lambda/2$ plate in front of the lens were used to control the intensity and the polarization axis of the pump beam, respectively. The lens was mounted on a translation stage in order to adjust the focus position in front of the gas cell. Without attenuation of the laser beam, a peak intensity of 6×10^{14} W/cm^2 can be reached in the laser focus. The pulse energy was reduced with the use of an iris aperture to avoid saturation of ionization in the Ar gas. Varying the intensity in a range below saturation enabled us to tune the spectral bandwidth of XUV pulses as shown in section 3.2. The cell had a length of 16 mm

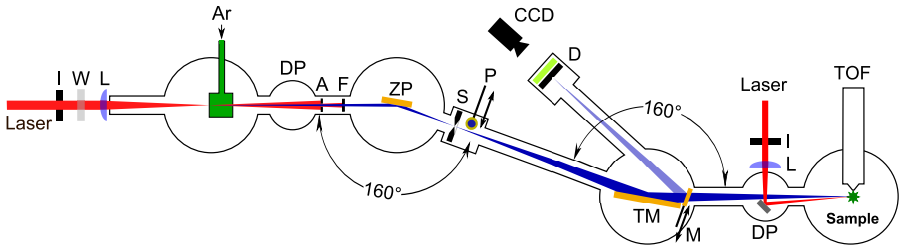

Fig. 1. Schematic view of the experimental setup. Notations: (I) Iris aperture, (W) wave plate, (L) lens, (DP) differential pumping stage, (A) aperture, (F) Al foil, (ZP) zone plate, (S) slit, (P) movable photodiode, (TM) toroidal mirror, (M) movable plane mirror, (D) position-sensitive detector, (TOF) time-of-flight electron spectrometer.

and was sealed with an aluminum foil into which the pump laser made the entrance and the exit apertures by itself. The argon pressure in the cell was adjusted by using a dosing valve to maximize the XUV photon flux which was detected with a calibrated photodiode behind the ZP monochromator. A typical pressure in the cell was 20 mbar during operation.

The ZP monochromator was positioned at a distance of 1000 mm from the HHG source. It consists of three gold-coated zone structures made on a single silicon substrate. The structures were designed to select the 17^{th}, 21^{st}, and 25^{th} harmonic of the pump beam, respectively. Details of their design will be given in a separate section below. The silicon substrate was mounted in a motorized stage that could be adjusted in three translational and three rotational directions with a precision of 0.1 μm and 2 μrad, respectively. A differential pumping stage enabled to maintain a low pressure of 10^{-8} mbar in the monochromator chamber during operation of the HHG source. A thin aluminum foil of 150 nm thickness was used in front of the ZPs to filter out the residual infrared (IR) pump beam. In order to prevent the foil from melting under the exposure of intense IR radiation, an aperture of 2 mm diameter was installed in front of the foil to block the main part of the pump beam. This aperture restricted the divergence of the XUV beam to 3.3 mrad in both transversal dimensions, resulting in a spot size of 3.3 mm of the incident beam at the ZP position.

In the monochromator, the harmonic of interest was deflected in the first diffraction order at an angle of 20° with respect to the incidence direction and was focused at a distance of 350 mm behind the ZP. Accordingly the 17^{th}, 21^{st}, and 25^{th} harmonics, respectively, were focused into the same spot when the center of the corresponding ZP was illuminated by the XUV light. A slit with an appropriate width, positioned at this focal point, was used to transmit only the desired harmonic since the other harmonics were reflected and focused differently. The slit width and its longitudinal and transversal positions with respect to the diffracted beam direction could be adjusted with micrometer precision.

A gold-coated toroidal mirror was used to refocus the divergent XUV beam into the interaction chamber equipped with a time-of-flight (TOF) electron spectrometer. The spectrometer characteristics are given in [29]. The refocussing mirror was mounted on a stage which, similar to the ZP stage, could be adjusted in three translational and three rotational dimensions. In order to minimize the focus aberrations, the focal length of the mirror was designed to refocus the beam with a magnification factor of 1 at the distance of 1200 mm, which is equal to the distance between the mirror and the slit. A plane gold mirror was inserted into the path of the refocused beam to monitor a replica of the XUV focus on a home-built position sensitive detector shown in Fig. 1. The detector is composed of a double stack of MCPs with a phosphor screen behind them and a CCD camera, which recorded light pulses from the phosphor screen at the detection

positions of XUV photons.

2.2. *Zone-plate monochromator*

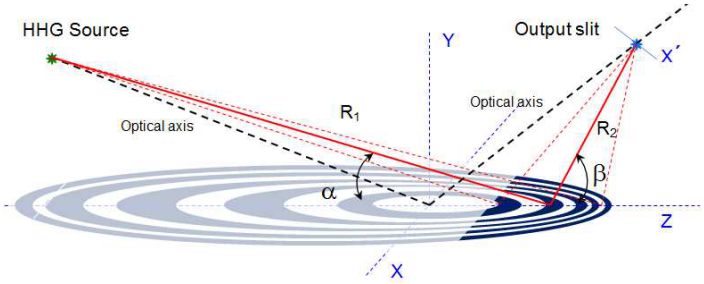

Fig. 2. Optical layout of the spectrometric element - reflection zone plate. The area of use is shown by deep blue color. See text for notations.

A simplified optical layout of the monochromator is shown in Fig. 2. Its central element possessing dispersion characteristics is the reflection zone plate, which represents a projection of the transmission Fresnel zone plate on the plane mirror surface [30]. As shown in Fig. 2, not the full elliptical lens structure is illuminated but only an off-axis section marked by deep blue color [31,32]. This off-axis section can be used as an ideal monochromator. Radiation incident onto this section is focused along the optical axis at high dispersion due to the high off-center mean line density. In addition, the specular reflex (zero-order reflection) can be easily separated and, most valuable for monochromatization, a slit in the plane perpendicular to the optical axis can be installed for the energy selection. The use of a mirror of high external reflectivity as a substrate for the ZP enables applications of this monochromator in a wide range of photon energies between 1 and 1500 eV, as it was first suggested in [33].

The energy dispersion ΔE in the ZP focal plane is defined by the relation [27]:

$$\frac{\Delta E}{\Delta x'} = \frac{E^2 d \sin\beta}{hcR_2} \quad , \tag{1}$$

where $\Delta x'$ represents the slit width in the focal plane, d is the local period of the zone structure in the middle of the illuminated area, β is the diffraction angle, R_2 is the distance from the ZP to the focal plane, h is the Plank constant, and c is the velocity of light. For a given spot size ΔS of the HHG source and a distance R_1 between the source and the ZP, the geometrical demagnification factor $M = R_2/R_1$ imposes the limitation to the minimum slit size:

$$\Delta x' > \Delta S/M \quad . \tag{2}$$

According to Eqs. (1) and (2), the energy resolution of a ZP monochromator is determined by the values of β, d, and $\Delta x'$. Equation (1) indicates that the value of $d\sin\beta$ is constant for a defined geometry of the HHG setup and a particular energy resolution $E/\Delta E$ desired in an experiment. A calculation procedure of the optimal structure period d is presented in [27]. For the first diffraction order of the ZP it has the form:

$$d = \frac{\lambda}{\sin\alpha}\left[\left(1+\cot^2\alpha+\left(\frac{R_2}{\Delta x'}\frac{\Delta E}{E}\right)^2\right)^{\frac{1}{2}} - \cot\alpha\right] \quad , \tag{3}$$

where λ is the radiation wavelength and α is the angle of incidence illustrated in Fig. 2.

In the present setup, the three ZPs designed for selection of the 17^{th}, 21^{st}, and 25^{th} harmonics, respectively, were fabricated on a single silicon substrate of 50 mm diameter by e-beam lithography and reactive ion etching. When a particular HHG photon energy has to be selected, the substrate can simply be moved along the x-axis in Fig. 2 to transfer the optical axis of the corresponding ZP into incident beam. This facilitates the alignment of the entire ZP assembly by monitoring the focus position of different harmonics while translating the assembly along the x-axis.

Table 1. The energy resolution and geometrical parameters of the HHG setup.

$E/\Delta E$	α°	β°	R_1 (mm)	R_2 (mm)
167	9.6	10.4	1000	350

The geometrical parameters of the HHG setup and the chosen energy resolution are summarized in Table 1. Taking the HHG source size of $\sim 100\ \mu$m and the geometrical demagnification factor $M = 2.86$ into account, the slit size in the focal plane of ZPs should be larger than $35\ \mu$m. The specifications of the individual ZPs are presented in Table 2. The meridional structure period d in the geometrical center of the ZP's operation area was determined for the three specific photon energies E by using Eq. (3) and the parameters given in Table 1. The ZP sections were manufactured with a length of 40 mm and a width of 4 mm. The optimal depth of the gold-coated structure profiles was calculated by using the program REFLEC [34]. In the energy range of 25 - 40 eV the optimal depth is in the order of 58 nm.

Table 2. Parameters of individual ZPs. d, d_1, and d_2 are the meridional structure periods in the geometrical center, at the low-density edge, and at the high-density edge of ZP's sections, respectively.

Harmonic	E (eV)	d_1 (μm)	d (μm)	d_2 (μm)
17	26.35	161.5	18.2	9.1
21	32.55	130.7	14.7	7.4
25	38.75	109.8	12.4	6.2

As mentioned in the introduction, the temporal broadening of the incident pulse is defined by the number N_s of illuminated structure elements. According to [35], for a ZP designed to select a particular harmonic of wavelength λ, this number can be expressed as $N_s = A^2/2F\lambda$, where A is the spot size of the incident beam and $F = R_1R_2/(R_1+R_2)$. Assuming a uniform intensity distribution over the XUV spatial beam profile, we obtain that the temporal broadening is $\Delta\tau_{\text{ZP}} = N_s\lambda/c = A^2/2cF$. With a spot size $A = 3.3$ mm this yields a value of 70 fs for the parameters of the present setup.

3. XUV pulse characterization

Results presented below were obtained with the use of the ZP designed for selection of the 21^{st} harmonic. Performance characteristics of the two other ZPs were found to be identical and therefore are not shown.

3.1. Spatial intensity distribution

Before assembling the entire setup, the XUV detector was positioned at the focal plane of the ZPs instead of the slit. Figure 3 shows an image of the intensity distribution of XUV radiation recorded at this position. The ZP designed for selection of the 21^{st} harmonic was used in

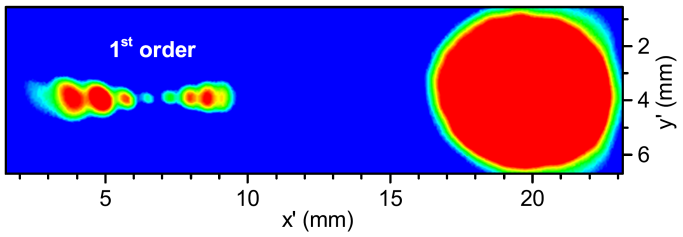

Fig. 3. Intensity distribution of XUV light in the slit plane. The image is recorded with the use of the zone plate designed to select the 21st harmonic. The large spot on the right hand side represents the unfocused specular reflex.

this measurement. The image clearly demonstrates the high-dispersion performance of the ZP, which can be seen on the left hand side of the image where the sequence of spots reveals contributions of different harmonics in the first diffraction order. The smallest spot in the middle of this sequence represents the signal of the 21st harmonic. It is well separated from contributions of other harmonics and from the unfocused specular reflex on the right hand side of the image. The 21st harmonic gives rise to a relatively weak signal in the image. This is because of saturation of the detector caused by the high flux density of XUV photons tightly focused onto the MCP.

Figure 3 also demonstrates the focusing property of the ZP. While the 21st harmonic is focused at the detector position into a small spot, other harmonics form larger spots in the image because their focuses lie either in front or behind the detector plane. Since the energy dispersion in the focal plane (given by the ZP design) and the energy interval between neighboring harmonics are constant, the larger spots partially overlap. Figure 3 shows that a slit of a few tenths of a millimeter width can be used in the focal plane to transmit the 21st harmonic only. Similar results were obtained for the other two ZPs designed to select the 17th and the 25th harmonics, respectively.

3.2. Spectral characteristics of selected harmonics

The spectral bandwidth of XUV pulses was measured by recording kinetic energy spectra of photoelectrons generated in the process of ionization of argon gas. XUV light was focused in the experimental chamber in front of the skimmer of the TOF spectrometer shown in Fig. 1. The spectrometer has a magnetic-bottle configuration. Its characteristics, such as the energy resolution and the collection efficiency of electrons, are presented in detail in [29]. The Ar pressure in the experimental chamber was maintained at 8×10^{-4} mbar during the data acquisition. Special efforts were made to verify that the recorded spectra are not affected by charge effects in the ionized medium.

Figure 4 shows a kinetic energy distribution of photoelectrons obtained with the use of the 21st harmonic. A slit size of 100 μm was used in this experiment. For comparison, a spectrum recorded with an open slit is shown in the inset. It demonstrates how the contribution of the neighboring harmonics can be eliminated by reducing the slit size without affecting transmission of the selected harmonic. For the spectrum shown in Fig. 4, the intensity ratio of the selected harmonic and the admixture of neighbouring harmonics is in the order of $1 : 6 \times 10^{-4}$.

Apart from the spectral bandwidth of the XUV pulse, the spectrometer resolution and the spin-orbit structure of the residual Ar^+ ions contribute to the width of the recorded energy peak of photoelectrons. The spin-orbit splitting of the ^{3}P state of Ar^+ is 0.177 eV [36]. This value is smaller than the energy resolution of the TOF spectrometer, which is in the order of 0.4 eV in the

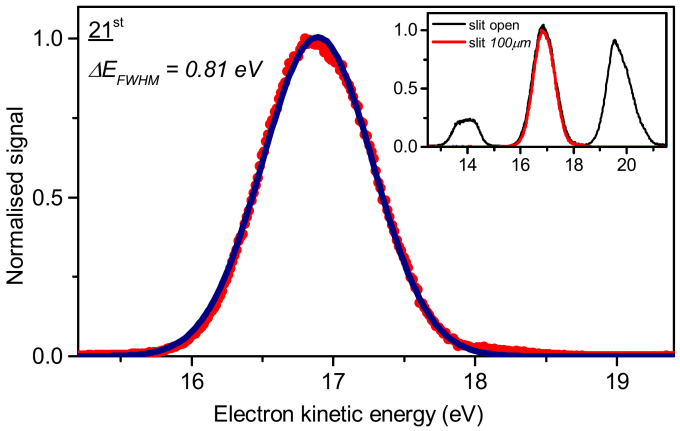

Fig. 4. Kinetic energy spectrum of photoelectrons generated by ionization of Ar with the use of the monochromatized 21st harmonic. The solid curve represents a fit of the measured spectrum to a sum of two Gaussian profiles associated with the spin-orbit structure of the residual Ar^+ ion. The inset displays a comparison of two photoelectron spectra recorded with a slit size of 100 μm and with an open slit, respectively.

considered kinetic energy range [29]. Therefore, the contributions of two ionization channels, associated with the generation of the residual ion in different spin-orbit states, are not resolved in the spectrum shown in Fig. 4. Considering the fine structure, the energy distribution was fit to a sum of two Gaussian profiles, lying at the fixed distance of 0.177 eV on the energy scale and having the same width which was a fit parameter. The fit yielded a value of 0.81 eV (FWHM) for the width. Taking the spectrometer resolution into account, we obtain that the spectral width of XUV radiation is 0.70 eV (FWHM). This spectral width was obtained with a pump intensity of 2.35×10^{14}W/cm^2. By reducing the latter to 1.5×10^{14}W/cm^2, the XUV bandwidth was decreased to 0.3 eV. This finding is in agreement with the recent results by He *et al.* in [18].

With the use of a stronger pump beam, the XUV photon flux was higher accordingly. For the 21st harmonic pumped with the intensity of 2.35×10^{14}W/cm^2, a flux of 10^9 photons per pulse was measured with a photodiode behind the monochromator.

3.3. Cross-correlation measurement of the XUV pulse duration

The pulse duration of XUV light was measured by means of a cross-correlation technique. It consisted in recording kinetic energy spectra of electrons generated in the process of IR-assisted ionization of Ar gas by XUV photons [22, 37, 38]. When the target atom is exposed to IR and XUV radiation at the same time, the ionization process can undergo a multiphoton transition where absorption of one XUV photon is combined with absorption or emission of several IR photons. The kinetic energy of the photoelectron can thus be expressed as

$$E_{\mathrm{kin}} = \hbar\omega_{\mathrm{XUV}} + N\hbar\omega_{\mathrm{IR}} - E_0 \quad , \tag{4}$$

where $\hbar\omega_{\mathrm{XUV}}$ and $\hbar\omega_{\mathrm{IR}}$ are photon energies of XUV and IR light, respectively, E_0 is the ionization potential of Ar, and $|N|$ represents the number of involved IR photons. The sign of N is positive or negative for ionization channels with absorption or emission of IR photons, respectively. For negative N, the number of emitted photons is constrained by the condition that the kinetic energy given by Eq. (4) should be positive.

The IR field needs to be sufficiently strong to initiate multiphoton transitions in the continuum spectrum of the parent atom. A criterion for the field strength was derived by Delone *et al.*

from a semiclassical analysis of dipole matrix elements for atomic continuum states [39]. According to this analysis, the continuum-continuum transitions are efficient if the laser intensity exceeds the value of $\omega_{IR}^{10/3}$ (in atomic units). Using this criterion, we obtain that for the Ti:sapphire laser frequency the critical intensity value is 2.5×10^{12} W/cm^2. On the other hand, the applied IR field should not deplete the population of Ar atoms in the interaction region due to the strong-field ionization process. The latter condition imposes an upper limit onto the intensity value. In previous cross-correlation experiments with the use of Ti:sapphire laser pulses of femtosecond duration, the peak IR intensity was restricted to a value below 10^{13} W/cm^2 [15,40]. At such intensities, the process of above-threshold ionization (ATI) of Ar in the IR field has a negligible yield at high electron kinetic energies and, thus, an overlap of the ATI spectrum with the cross-correlation spectrum is avoided as well.

In the present setup, the IR pulse energy was controlled with the use of an iris aperture positioned in front of a lens of 400 mm focal length which focused the IR beam into the region of overlap with the XUV beam (see Fig. 1). The IR peak intensity in the interaction region is estimated to be in the order of 1.7×10^{12} W/cm^2. The time delay between the XUV and the IR pulses was varied with the use of an optical delay stage installed in the IR beam path. The delay could be controlled with a precision of 0.5 fs. Since the IR beam was passing through the beam splitter used to split the laser output and the HHG pump beam was the the reflected part, a plane glass window of an appropriate thickness was used in the path of the HHG pump beam to compensate for dispersion in the splitter. The laser compressor was tuned for the shortest temporal width of the cross correlation signal. The actual IR pulse duration of 25 fs in the interaction region was measured by using a SPIDER device.

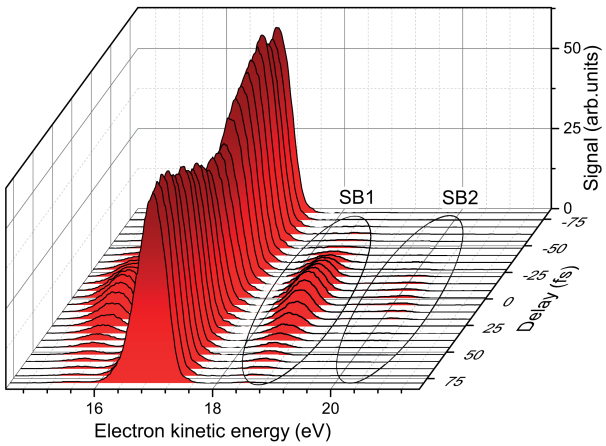

Fig. 5. IR-assisted ionization of Ar by XUV light of the 21st harmonic. Series of photoelectron energy spectra are recorded at different time delays between the XUV and the IR pulses. The IR peak intensity is in the order of 1.7×10^{12} W/cm^2.

Figure 5 shows a series of kinetic energy spectra obtained with the use of the 21st harmonic at different time delays between the XUV and the IR pulses. These results were obtained with the reduced HHG pump intensity of 1.5×10^{14}W/cm^2. Each spectrum was recorded with the same acquisition time and at fixed experimental parameters such as the laser intensity and the gas pressure. The appearance of several sidebands (SB) at small delays and at both sides from the central peak can be seen in the figure. Their amplitudes and temporal widths monotonically decrease with the increase of the SB number. For a quantitative analysis of the cross correlation

signal, the electron yield was integrated over the energy peak of each SB. The dependency of the integrated yield as a function of the time delay is shown in Fig. 6.

For reduced IR intensities applied in the present experiment, one can use the pertubation theory to describe the cross correlation signal. Considering a multiphoton process that involves absorption of one XUV photon and absorption or emission of number $|N|$ of IR photons, the ionization rate is proportional to the product $I_{\mathrm{XUV}} I_{\mathrm{IR}}^{|N|}$, where I_{XUV} and I_{IR} are intensities of XUV and IR radiation, respectively. Thus, the ionization yield $S_N(\tau)$ in the N^{th} SB at a given time delay τ is proportional to the integral

$$S_N(\tau) \propto \int_{-\infty}^{+\infty} I_{\mathrm{XUV}}(t) I_{\mathrm{IR}}^{|N|}(t-\tau) dt \quad . \tag{5}$$

Assuming that the XUV and the IR pulses have Gaussian temporal envelopes $\exp(-t^2/\tau_{\mathrm{XUV}}^2)$ and $\exp(-t^2/\tau_{\mathrm{IR}}^2)$, respectively, from Eq. (5) we obtain that the cross-correlation signal has the Gaussian shape

$$S_N(\tau) \propto \exp(-\tau^2/\tau_N^2) \quad , \tag{6}$$

where

$$\tau_N^2 = \tau_{\mathrm{XUV}}^2 + \frac{\tau_{\mathrm{IR}}^2}{|N|} \quad . \tag{7}$$

Here τ_{XUV} and τ_{IR} represent the Gaussian widths of the XUV and the IR pulses, respectively. Equation (7) demonstrates that the temporal width τ_N of the cross correlation signal is decreasing with the increase of the SB number and converges to the value of the XUV pulse duration in the limit of large positive or negative N.

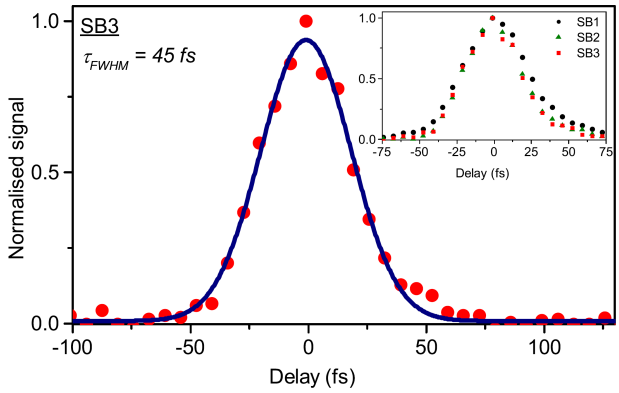

Fig. 6. Integrated cross-correlation signal in the third sideband (circles). The solid line represents a Gaussian fit to the experimental data points. The inset shows a comparison of the integrated signals of the first, the second, and the third sideband, demonstrating the convergence of the cross correlation temporal width with the increase of the sideband number.

The temporal dependencies of the cross-correlation signal in the three SBs shown in the inset of Fig. 6 were fitted to the Gaussian profile described in Eq. (6) with τ_N as a fit parameter. The obtained values of τ_N were used to calculate the full widths at half maximum of the cross correlation temporal profiles as $\tau_N^{\mathrm{FWHM}} = 2\sqrt{\ln 2}\tau_N$. This yielded values of 54 fs, 46 fs, and 45 fs for the first, the second, and the third sideband, respectively. The value of τ_N^{FWHM} converges to approximately 45 fs for an increasing SB number, which represents the XUV pulse duration achieved in the present setup.

The measured pulse duration is given by a convolution of the XUV pulse length before monochromatization with the temporal broadening caused by the ZP monochromator. Assuming the generated XUV pulse duration is in the order of the pump pulse length, we obtain that the time distortion of the ZP is approximately 37 fs. This value is smaller than the initially calculated pulse dispersion of 70 fs. The difference originates from the assumption that the ZP structure is illuminated by a XUV beam with a uniform spatial intensity distribution.

4. Summary

We presented results of the first practical implementation of a ZP-based monochromator to select femtosecond XUV light pulses generated in the HHG process. Excellent performance characteristics are achieved for both the time and the energy resolution of the monochromator. In the present setup, a single harmonic is selected with a pulse duration of 45 fs, corresponding to a temporal broadening of approximately 37 fs due to the ZP's optical dispersion. This value can be minimized further by reduction of the aperture size of the incident HHG beam.

One should emphasize that the ZP monochromator consists of a single optical element that combines reflection, focusing and dispersion properties together. Therefore, it has a much higher transmission efficiency compared to a multi-element monochromator. The single-element feature also simplifies handling of the XUV beam.

The ZP sections of the monochromator are designed for selection of a desired harmonic with the optimal combination of the energy and the time resolution. Therefore, the performance of this instrument is superior to a grating monochromator where the density of groves is fixed. Moreover, by making the ZP sections long, the balance between the energy and the time resolution can be varied within a single ZP section while using its different parts with different density of the structure elements. This provides flexibility in the application of a ZP-based monochromator.

In the present work we focused on the performance characteristics of a monochromator consisting of a single zone plate. We did not consider the XUV pulse compression with the use of an additional dispersive element, which was demonstrated by Poletto *et.al.* in [22]. Implementation of a second ZP to achieve a transform-limited duration of a HHG pulse represents an interesting task for further development of the setup.

Acknowledgments

This work is funded by the European Research Council, Grant No. 279344 (E.F.A.), and by the Helmholtz-Gemeinschaft via the VH-NG-635 Grant (E.F.A.). The authors acknowledge support by the BMBF, Project 05K12CB4 "Next generation instrumentation for ultrafast X-ray science at accelerator-driven photon sources" and a Marie Curie FP7-Reintegration-Grants within the 7th European Community Framework Program (project No. PCIG10-GA-2011-297905). Discussions with Prof. Bernd Abel and his co-workers are greatly appreciated.